DCM Control Method of Boost Converter based on Conventional CCM Control

Le Hoai Nam, Koji Orikawa, Jun-ichi Itoh
Department of Electrical, Electronics and Information Engineering
Nagaoka University of Technology
Nagaoka, Japan
lehoainam@stn.nagaokaut.ac.jp

***Abstract*— This paper proposes current control method for DCM to achieve same control performance as CCM. The proposed control loop is designed based on the conventional current control loop in CCM. By using only one PI controller and introduction of two correction factors, the proposed control method can control both CCM and DCM current exactly to design values. In this paper, the operation of the proposed control method is confirmed by simulation and experiment. The simulation results of the current response in both CCM and DCM agree with design values. In the experimental results, due to the delay in feedback, error 11.3% in rise time and error 2.5 point in overshoot occur. Furthermore, the voltage regulation experiment with the proposed current controller as a inner control loop is conducted. As load varies, the recovery time for the output voltage regulation is about 20 ms and the overshoot – undershoot voltage is below 3%.**

I. INTRODUCTION

The research in electric power conversion has grown rapidly in recent years due to energy crisis. DC-DC converters present in most power conversion systems or devices such as: fuel cell systems in mobile devices [1], photovoltaic(PV) systems [2], lithium-ion battery in hybrid vehicles (HEVs) [3][4], smart power system for servers [5], e.t.c. Because the minimization of those DC-DC converters not only increases the mobility of mobile devices but also simplifies the layout for PV systems or battery systems in HEVs, many studies have focused on shrinking the DC-DC converter circuit as much as possible. Besides, passive components such as inductors and capacitors account for the majority of the volume of DC-DC converters, so the miniaturization of these passive components leads to compact DC-DC converter generation. One of methods to minimize these passive components is to switch the circuit at high frequency [6]. However, switching at high frequency leads to the increase of frequency-dependent losses such as switching loss in MOSFET or recovery loss in diode [7]. The increase of conversion loss accounts for larger cooling sink, and this makes the minimization of DC-DC converters further difficult. In order to eliminate the increase of loss when switching at high frequency, the concept of resonant converters has been proposed [8]. Some researchers have introduced DC-DC converters operating at frequencies of hundreds of MHz, while maintaining the power conversion efficiency high [9][10]. However, in those resonant converter, because switch's duty is limited in narrow range, the problems such as the uncontrollability of output voltage or the overheat when resonant converter operates in boot mode [11], are difficult to be solved. This limits the practical applications for resonant converters. On the other hand, the minimization of the inductor can be accomplished by the utility of Discontinuous Current Mode (DCM).

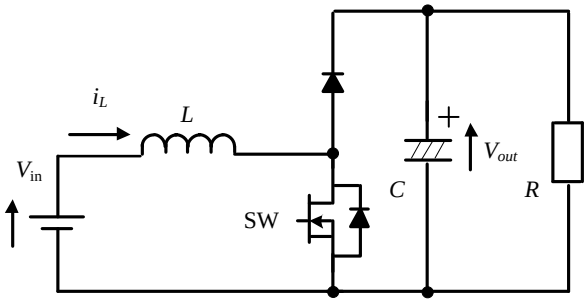

Fig. 1. A unidirectional boost converter

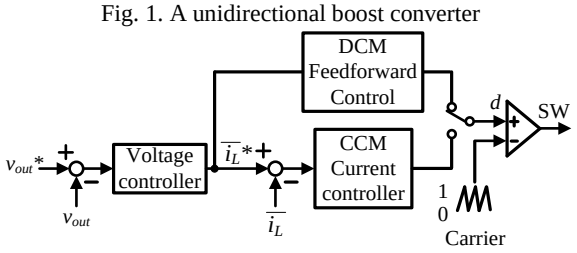

Fig. 2. Conventional CCM/DCM control method.

Fig. 1 shows a unidirectional boost converter which is generally applied in PV system to regulate the output voltage while preventing the power from flowing back into the input side. When the inductor is minimized, the ripple of the input current becomes higher, and this leads to the discontinuity of input current. This can be understood that only a small amount of energy can be stored in a minimized inductor, so all stored energy in inductor will be released before a new switching period begins. In order to design controller for DCM similar to the conventional Continuous Current Mode (CCM), many researches have been conducted [12][13][14], but a specific method to accomplish this has not been discussed.

Furthermore, the inductor current alternates between CCM and DCM depending on the variation of the load, and this likely leads to the unstable operation of the converter. Many CCM/DCM control methods have been studied in past years to deal with the nonlinearity in DCM, such as Adaptive Tuning method [15], Bi-frequency Pulse-Train Control technique [16], Peak Current Mode Bifrequency Control Technique [17], Current-Mode

Synthetic Control Technique [18], Switching-Frequency Control [19], e.t.c [20][21][22]. However, those control methods either lead to the complication of the control system, or the increase in cost for the auxiliary circuit such as the variable frequency pulse generator.

Fig. 2 shows a conventional control system which composes of an Automatic Voltage Regulator (AVR) and two Automatic Current Regulators (ACR) [23]. Many designers prefer to utilize PI controller for both AVR and ACR because of its simple design. In conventional inductor current PI control method, the PI parameters for CCM can be designed simply based on the linear CCM transfer function. On the other hand, due to the nonlinear characteristic of the DCM transfer function, the current control loop in DCM is designed based on the reduced-order model [12][23]. This leads to the feed forward current control in DCM. As a result, the DCM current response cannot be controlled as same as the CCM current response. In this case, DCM current control is effective in only critical conditions.

This paper proposes a control method in which only one PI controller is necessary to regulate both CCM and DCM. By introduction two correction factors into the conventional inner current control loop in CCM, the current response of DCM is controlled exactly to that of CCM. Besides, it is not necessary to detect the current mode. In this paper, first, the principle of the proposed CCM-DCM control method is described. Second, the introduction of two correction factors α_{DCM} and K_{DCM} are described. Then, the transition between CCM and DCM is explained. Finally, the operation of the boost converter which the proposed control method is applied, is confirmed by simulation and experiment.

II. PROPOSED CCM-DCM CONTROL SCHEME

A. Conventional inner current loop design in CCM

Fig. 3 shows typical boost converter configuration. The average small signal modeling technique is used to model the boost converter for the inner current control loop design [6]. In this chapter, the output voltage is assumed to be constant, because the response of the inductor current is much higher than that of the output voltage in ACR design step.

Fig. 4 shows inductor current waveform in DCM, where d and d' denote the duty ratio of the first and the second interval respectively. Equation based on the average model of the boost converter in CCM and DCM is given by (1),

$$L\frac{d\bar{i}_L}{dt} = dV_{in} + d'(V_{in} - V_{out}) \quad \text{.....(1)}$$

where V_{in} is the input voltage, V_{out} is the output voltage, $\bar{i}_L$ is the average inductor current during a switching period T_{sw}, and L is the inductance. In case of CCM, the relationship between d and d' is given by (2).

$$d + d' = 1 \quad \text{.....(2)}$$

Substituting (2) into (1), (3) is obtained.

$$L\frac{d\bar{i}_L}{dt} = V_{in} - V_{out} + dV_{out} \quad \text{.....(3)}$$

Here, the averaged control to inductor current transfer

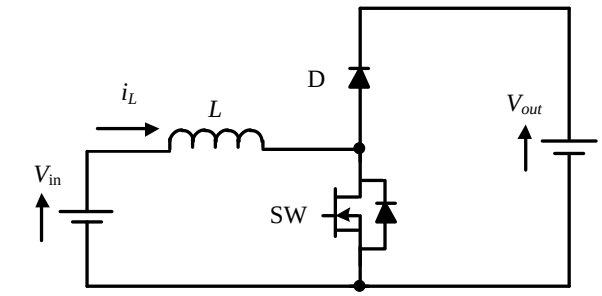

Fig. 3. Typical boost converter configuration in ACR design

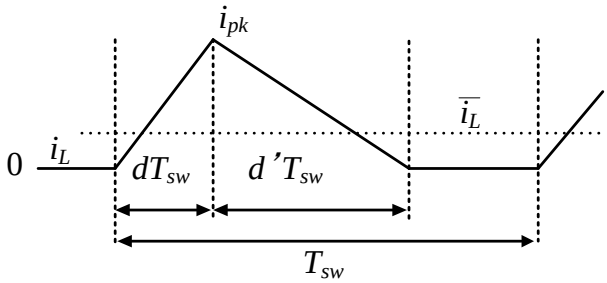

Fig. 4. Inductor current waveform in DCM

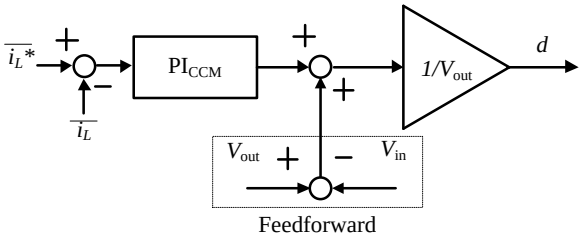

Fig. 5. Conventional inner current loop in CCM

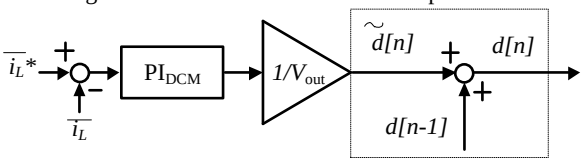

Fig. 6. Proposed inner current loop in DCM

function in CCM is given by (4),

$$G_{CCM}(s) = \frac{\bar{i}_L(s)}{d(s)} = \frac{V_{out}}{sL} \quad \text{.....(4)}$$

Fig. 5 shows ACR-CCM designed based on (3) and (4). The integral period T_i and proportional gain K_p of PI$_{CCM}$ controller are designed based on the second-order standard form (5),

$$G_{2nd-order-delay}(s) = \frac{\omega_n^{\,2}}{s^2 + 2\zeta\omega_n s + \omega_n^{\,2}} \quad \text{.....(5)}$$

where ω_n is the natural angular frequency, ζ is the damping factor, and both of which are designed to achieve the desired inductor current response. The closed loop transfer function of ACR-CCM is derived by (6).

$$H_{CCM-ACR}(s) = \frac{\bar{i}_L(s)}{\bar{i}_L{}^*(s)} = \frac{\frac{K_p}{LT_i}(1+sT_i)}{s^2 + \frac{K_p}{L}s + \frac{K_p}{LT_i}} \quad \text{.....(6)}$$

In order to make the design of PI parameters simple, a low pass filter whose role is to filter the command current $\bar{i}_L{}^*$ is necessary for matching (5) and (6). However, a low pass filter is not essentially needed.

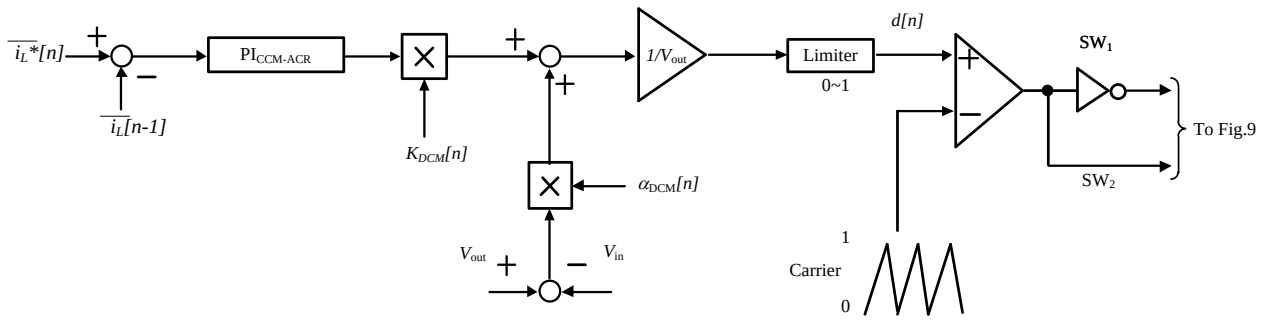

Fig. 7. Configuration of the proposed CCM/DCM current controller.

Using a low pass filter depends on designers. The PI parameters are then obtained by matching (5) and (6).

$$K_p = 2\xi\omega_n L \quad \text{.....(7)}$$

$$T_i = \frac{2\xi}{\omega_n} \quad \text{.....(8)}$$

B. Small signal modeling in DCM

In case of DCM, the relationship between d and d' is given by (9).

$$d + d' < 1 \quad \text{.....(9)}$$

In order to derive the averaged control to inductor current transfer function in DCM, it is necessary to represent the second interval d' in Fig. 4 as a function of the first interval d. Based on [12] and the waveform shown in Fig. 4, this can be done as follow

$$\bar{i}_L = \frac{i_{pk}}{2}(d + d') \quad \text{.....(10)}$$

where i_{pk} is the inductor peak current during a switching period T_{sw}. Neglect the voltage drop by the switch, the voltage across the inductor during the first interval d can be assumed as V_{in}. The inductor peak current can be written as

$$i_{pk} = \frac{V_{in}}{L} dT_{sw} \quad \text{.....(11)}$$

Substituting (11) into (10) and solving the resulting equation for d' yields

$$d' = \frac{2L\bar{i}_L}{dT_{sw}V_{in}} - d \quad \text{.....(12)}$$

Substituting (12) into (1), (13) is obtained.

$$L\frac{d\bar{i}_L}{dt} = \frac{2L\bar{i}_L}{dT_{sw}}\left(\frac{V_{in} - V_{out}}{V_{in}}\right) + dV_{out} \quad \text{.....(13)}$$

In case of DCM, the averaged control to inductor current transfer function in DCM cannot be derived simply from (13) because of its nonlinearity compared to (3). Therefore, (13) is linearized at steady point, then the averaged control to inductor current transfer function in DCM can be derived by linearized equation (14)

$$G_{DCM}(s) = \frac{\tilde{i}_L(s)}{\tilde{d}(s)} = \frac{V_{out}}{L} \frac{2}{s + 2\sqrt{\frac{(V_{out}/V_{in} - 1)V_{out}}{2LI_L T_{sw}}}} \quad \text{.....(14)}$$

where $\tilde{i}_L$ is the small signal of inductor current, $\tilde{d}$ is the small signal of duty, I_L is the value of the inductor current at steady point. Eq. (14) indicates that not only the gain of the DCM transfer function differs from that of the CCM transfer function, but also the control target changes from the full values $\bar{i}_L$ and d in CCM into the small values $\tilde{i}_L$ and $\tilde{d}$ in DCM. Therefore, in order to achieve the DCM current control by the conventional CCM-ACR, both the control gain and the control target of the PI$_{CCM}$ controller needs to be modified. The modification of control target and control gain is achieved by introducing two corrector factors α_{DCM} and K_{DCM} into conventional current control loop in CCM.

C. Proposed CCM/DCM current control loop

1) Derivation of the first correction factor α_{DCM}

The modification of the control target from CCM to DCM is achieved by compensating the output of the CCM feedforward part using the correction factor α_{DCM} that given in (16) [22]. The procedure to calculate this correction factor α_{DCM} is as follows.

When considering the control system in z-domain, the control target of DCM $\tilde{d}[n]$ is given by

$$\tilde{d}[n] = d[n] - d[n-1] \quad \text{.....(15)}$$

where $d[n]$ is the output duty to control inductor current, $d[n-1]$ is the value of the duty in one sampling period before. Eq. (15) indicates that, the output duty is the sum between the value of the duty in one sampling period before and the difference duty controlled by the PI controller in DCM.

Fig. 6 shows the proposed DCM current control loop. The objective to change Fig. 5 into Fig. 6, is achieved by multiplying the output of the CCM feedforward part with the correction factor α_{DCM}.

$$\alpha_{DCM}[n] = \frac{V_{out}}{V_{out} - V_{in}} d[n-1] \quad \text{.....(16)}$$

2) Derivation of the second correction factor K_{DCM}

The modification of the control gain from CCM to DCM is achieved by compensating the output of the PI$_{CCM}$ using the correction factor K_{DCM} that given by (21). The procedure to calculate this correction factor K_{DCM} is as follows.

The discretized control gains (17), (18) are obtained by discretizing (4) and (14) in sampling period T_{sw}. Note that the sampling period equals to the switching period.

$$\left|G_{CCM}(z)\right| = \frac{V_{out}T_{sw}}{L} \quad \text{.....(17)}$$

$$\left|G_{DCM}(z)\right| = \frac{V_{out}}{L}\sqrt{\frac{2LI_L T_{sw}}{(V_{out}/V_{in} - 1)V_{out}}} \quad \text{.....(18)}$$

In order to change the control gain from $|G_{CCM}(z)|$ to

$|G_{DCM}(z)|$, a correction factor K_{DCM} is multiplied with the output of the PI_{CCM} controller. K_{DCM} is given by (19).

$$K_{DCM} = \frac{|G_{CCM}(z)|}{|G_{DCM}(z)|} = \sqrt{\frac{(V_{out}/V_{in}-1)V_{out}T_{sw}}{2LI_L}} \quad \text{..... (19)}$$

The K_{DCM} in (19) is simplified by using the equation of I_L at steady state as below [12]. Note that (20) is obtained by simply let the inductor current differential part $\frac{d\bar{i}_L}{dt}$ in (13) be zero.

$$I_L = \bar{i}_L[n-1] = \frac{d^2[n-1]T_{sw}V_{out}V_{in}}{2(V_{out}-V_{in})L} \quad \text{.....(20)}$$

Substituting (20) into (19), K_{DCM} is also given by (21).

$$K_{DCM}[n] = \frac{V_{out}-V_{in}}{V_{in}}\frac{1}{d[n-1]} \quad \text{.....(21)}$$

Fig. 7 shows the proposed CCM-DCM current control loop, which controls both CCM and DCM by using only one PI_{CCM} and two correction factors α_{DCM} and K_{DCM}.

Table I shows the values of two correction factors in case of CCM and DCM.

D. Transition between CCM and DCM

As mentioned above, the proposed control method can achieve both CCM and DCM control without detect the inductor current. The approach for this can be explained as follow. From Table I , both correction factors α_{DCM} and K_{DCM} have to be set to 1 when the circuit operates in CCM and be set to (16) , (21) respectively in DCM.

Fig. 8 shows two correction factors α_{DCM} and K_{DCM} as functions of duty d. Let consider the transition of α_{DCM} first. As shown in Fig. 8, the transition point falls right into the boundary between CCM and DCM, which means α_{DCM} can trade between CCM value and DCM value without detecting the circuit operating mode. This can be explained as when the circuit operates in CCM , the duty d follows as

$$d = \frac{V_{out}-V_{in}}{V_{out}} \quad \text{.....(22)}$$

Neglect the parasitic characteristic of switch and diode, (22) is always established whenever the circuit operates in CCM. Substituting (22) into (16), it is understood that α_{DCM} is set to 1 because of the steady operation of CCM.

On the other hand, as shown in Fig. 8, K_{DCM} do not change into 1 automatically when the circuit has already switched from DCM to CCM. However, because α_{DCM} can change states automatically, the transition of K_{DCM} is accomplished by observing the value of α_{DCM}. To be specific, whenever α_{DCM} becomes 1, K_{DCM} is also set to 1, otherwise K_{DCM} follows as (21). Because α_{DCM} can trade values between CCM and DCM without detecting current mode, the transition of K_{DCM} based on α_{DCM} state is also accomplished without sensing which mode the circuit is operating.

III. SIMULATION RESULTS

Simulation are carried out to verify the proposed CCM/DCM control method.

Fig. 9 shows the simulation system. The switching device in the upper arm SW_1 is used when the boost converter operates in CCM. When the DCM operation is tested, the switch SW_1 is always kept at off-state.

TABLE I
VALUES OF TWO CORRECTION FACTOR IN CCM AND DCM

Current Mode	CCM	DCM
α_{DCM}	1	$V_{out}d[n-1]/(V_{out}-V_{in})$
K_{DCM}	1	$(V_{out}-V_{in})/(V_{in}d[n-1])$

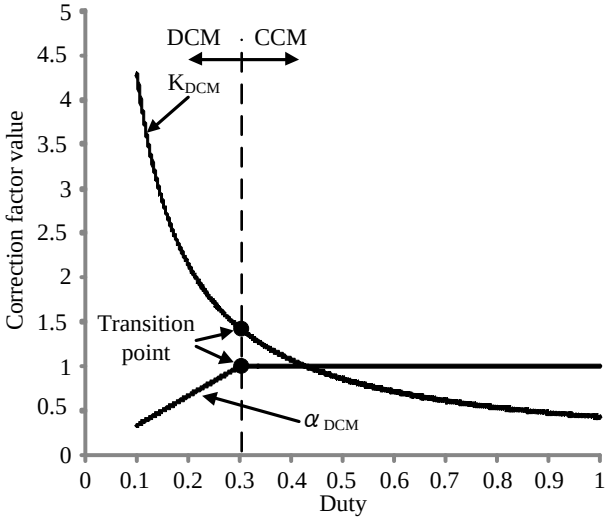

Fig. 8. Relationship between duty and correction factors at steady point

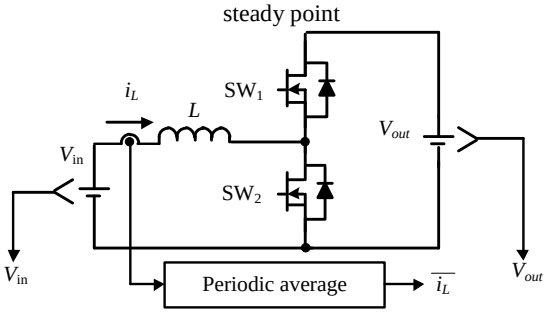

Fig. 9. Boost converter for ACR Simulation and Experiment.

TABLE II
SIMULATION AND EXPERIMENTAL PARAMETERS

Input voltage V_{in}	70 V
Output voltage V_{out}	100 V
Rated output power P_{out}	56 W
Boost chopper inductor L	360 μH
Switching frequency f_{sw}	20 kHz
Sampling frequency f_{samp}	20 kHz
Damping factor ζ ACR	0.7
Natural angular frequency ω_n ACR	2500/3000/3500 rad/s

Table II lists the system parameters and ratings. In order to avoid the appearance of the delay time in feedback, the sampling of the average inductor current is achieved by simply taking advantage of the periodic average block in simulator.

Fig. 10 shows the simulation results of the step response. Fig. 10(a) and Fig. 10(b) show the current waveform of CCM and DCM respectively. Fig. 10(c) shows the step response of the average inductor current in both CCM and DCM. It can be concluded from Fig. 10(c) that the DCM current response is the same as the CCM current response. In order to verify the operation of the proposed CCM-DCM control method in many cases, the measurement of the overshoot and the rise time of the current response are conducted while varying the natural

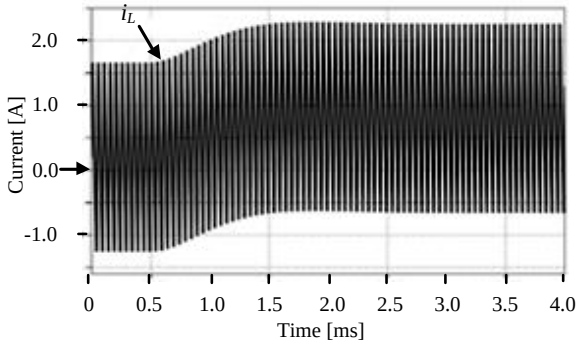

(a) CCM current waveform.

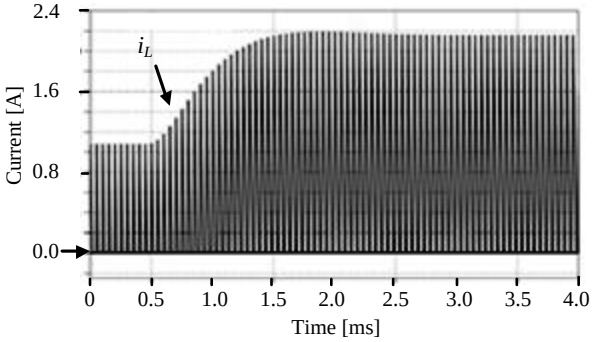

(b) DCM current waveform.

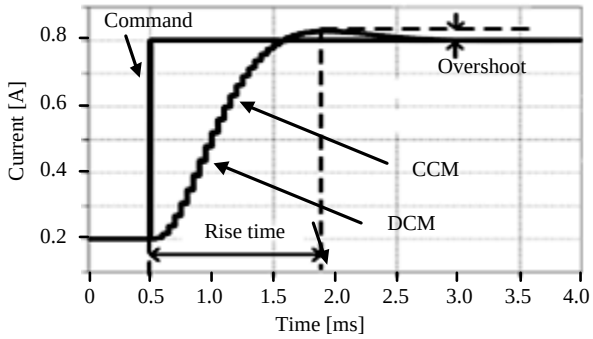

(c) CCM and DCM average current response

Fig. 10. Simulation results of step response.

frequency of the PI_{CCM} controller.

Fig. 11 shows the overshoot and the rise time of the current response in simulation while varying the natural frequency of the PI_{CCM} controller. It is confirmed that the rise time and the overshoot of both CCM and DCM current are agreed with the design values.

IV. Experimental results

The experimental conditions are the same as those of the simulation as shown in Table II. In experiment, the average inductor current is sampled by using a Low Pass Filter (LPF) with cutoff frequency of 2 kHz. Note that the switch SW_1 is always kept at off-state in case of DCM.

Fig. 12 and Fig.13 show the experimental step response of the inductor current response at ω_n = 3000 rad/s and ω_n = 3500 rad/s, respectively. Both the inductor current and the average values of the inductor current in CCM and DCM are demonstrated in same waveform. There is a slight difference in the shape of the current response between CCM and DCM. This difference can be explained as follows. The state of SW_1 is different between CCM and DCM. As a result, the on-resistance in

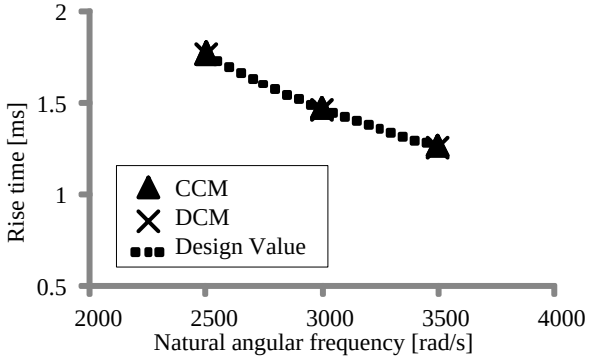

(a) Rise time.

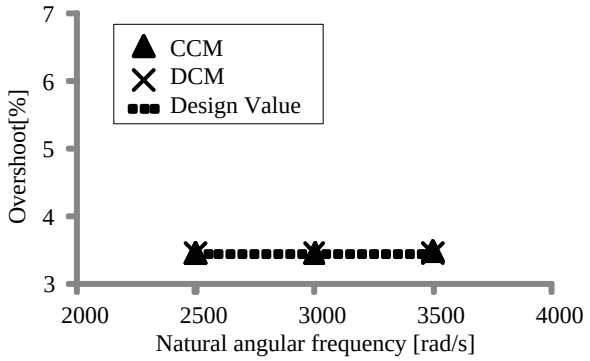

(b) Overshoot.

Fig. 11. Rise time and overshoot of the current response in simulation.

MOSFET and the voltage drop by diode change the shape of the current response.

Fig. 14 shows the overshoot and the rise time of the current response in experiment while varying the natural frequency of the PI_{CCM} controller. There are errors between CCM/DCM current response and the design values. In the rise time results, the maximum error is 11.3%, while it is 2.5 point in the overshoot results. It can be seen from Fig. 13 that in both CCM response and DCM response, the experimental results of the rise time tend to become smaller than the design values, while the experimental results of the overshoot tend to become higher than design values. This error tendency can be explained as follows. When a LPF is used to obtain the average values of any signal, the time constant in LPF becomes the delay time between the input and output of LPF. This delay time increases the total delay time in the feedback of the controller. As a result, the rise time of the system response becomes shorter, while the overshoot becomes higher than the design values. Next step is to confirm the validity of the proposed CCM/DCM current controller in the output voltage regulation system.

Fig. 15 shows the boost converter whose the output voltage needs to be regulated for proper operation . Note that the upper switch is changed into a diode in order to let the circuit operate in DCM at light load. This also prevents the current flowing back into the source, which damages the source in such PV systems. Besides, the PI parameters in AVR are as follows

$$K_p = 2\xi\omega_n C \quad \text{.....(23)}$$

$$T_i = \frac{2\xi}{\omega_n} \quad \text{.....(24)}$$

Table III lists the system parameters and ratings in

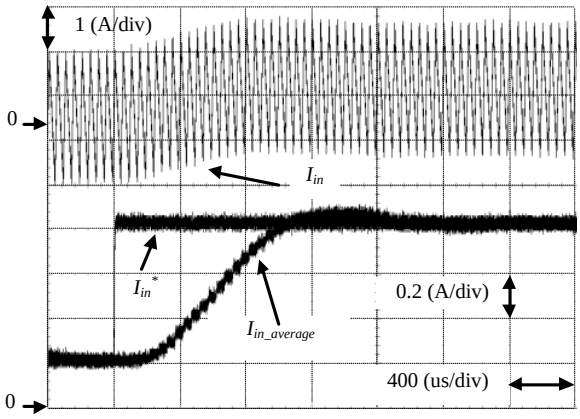

(a) CCM current waveform and average current response.

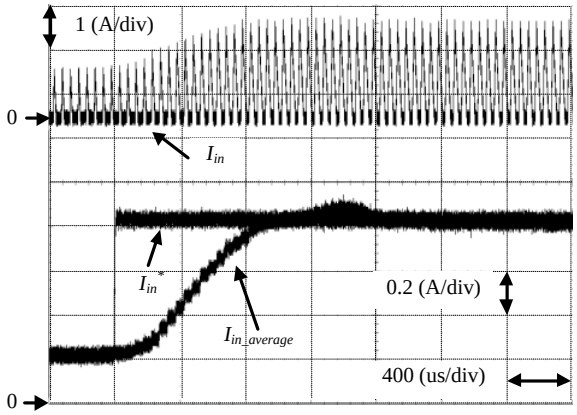

(b) DCM current waveform and average current response.

Fig. 12. Experimental results of step response (ω_n = 3000 rad/s)

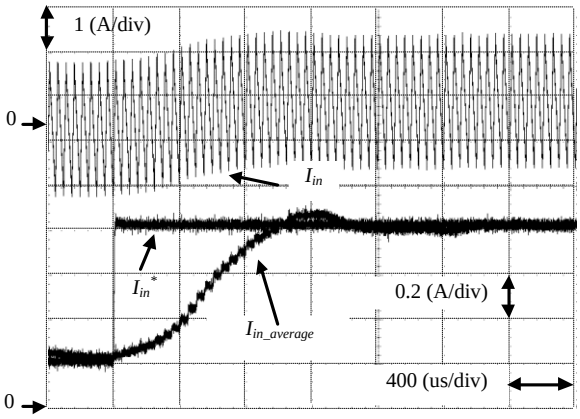

(a) CCM current waveform and average current response.

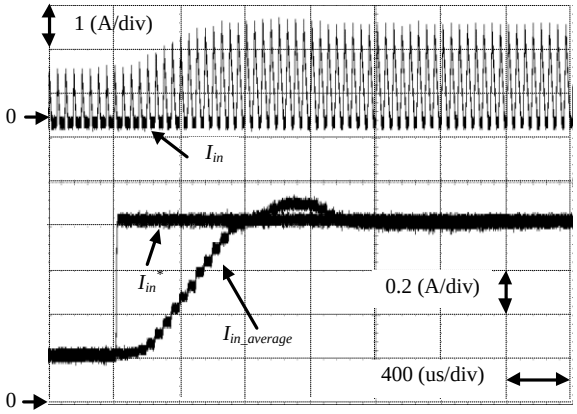

(b) DCM current waveform and average current response.

Fig. 13. Experimental results of step response (ω_n = 3500 rad/s)

AVR experiment. Note that the natural angular frequency in AVR should be designed smaller at least 10 times than that of ACR in order to achieve the stable operation of the control system.

Fig. 16 shows the experiment results of load transient response between CCM (heavy load) and DCM(light load). Fig. 16(a) shows the output voltage response and the input current response when load varies from 40% in DCM to 100% in CCM. The recovery time for the output voltage regulation is about 20 ms and the undershoot voltage is 2 V, which is below 3% of the output voltage. Fig. 16(b) shows the output voltage response and the input current response when load varies from 100% in CCM to 40% in DCM. The recovery time for the output voltage regulation is about 20 ms and the overshoot voltage is 2 V, which is below 3% of the output voltage. There are two things needs to be noted in Fig. 16. First, when load varies the input voltage also slightly changes. In the experiment, a three-phase diode bridge rectifier and an input side smoothing capacitor are applied as the voltage source, so when the load varies, the voltage drop by the diode bridge and the smoothing capacitor also changes. This results in the variation of the input voltage when the load varies. Second, the input current quite oscillates not only in DCM but also in CCM. This is explained that, the accuracy of the average input current sampling mainly depends on three factors: the ripple of the input current, the speed of the D/A converter, and the time constant of LPF. According with the minimization

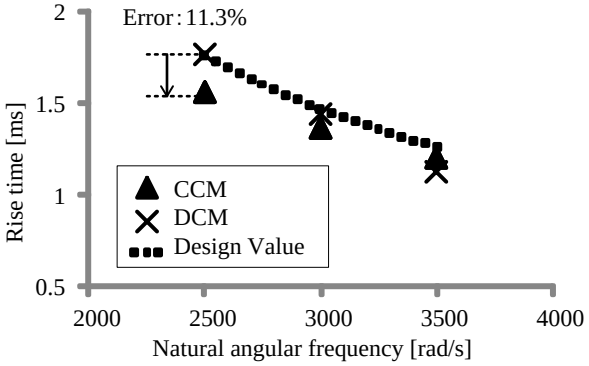

(a) Rise time.

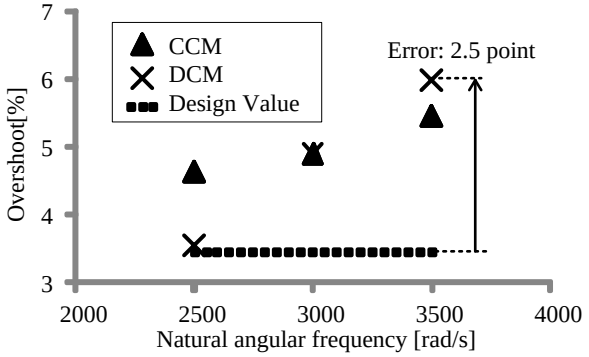

(b) Overshoot.

Fig. 14. Rise time and overshoot of the current response in experiment

of the boost chopper inductor, the ripple current becomes higher. The average value of the input current needs to be sampled in order to achieve the proper operation of ACR. Therefore, a LPF is applied in order to obtain average value of the input current. However, this LPF introduces a considerable delay time into the feedback, while the mismatch in each sampling point in the D/A converter lead to the feedback into ACR is just a delayed value of the actual current. This results in the oscillation of the input current. However, in both cases, the output voltage is regulated at the command. On the other hand, in order to avoid the oscillation of duty in CCM which might cause the current mode determination inaccuracy, instead of comparing with 1, α_{DCM} is compared with 0.9 to determine the state of K_{DCM} . This achieves the CCM/DCM current control without detecting the input current or the parameters of the boost converter circuit.

Fig. 17 shows the experiment results of load transient at light load. Fig. 17(a)(b) shows the output voltage response and the input current response when load varies from 20% in DCM to 40% in CCM and vice versa. The recovery time for the output voltage regulation is about 15 ms and the overshoot voltage is least than 1 V, which is below 2% of the output voltage. Both Fig. 16 and Fig. 17 confirm the validity of the proposed CCM/DCM current control method.

V. Conclusion

In this paper, a control method for both CCM and DCM was proposed. In the proposed method, the control of CCM and DCM current is achieved by using only one PI controller and introduction of two correction factors. Besides, the CCM/DCM current control can be achieved without sensing the input current or any circuit parameters. Therefore, the simplification of the CCM/DCM control system is possible. The validity of the proposed current control is confirmed by both simulation and experiment.

Future works will be focused on designing the minimized inductor and evaluating the conversion efficiency.

References

[1] Koji Orikawa, Jun-ichi Itoh: "A comparison of the series-parallel compensation type DC-DC converters using both a fuel cell and a battery", IEEE ECCE 2010, pp.1428-1435, 2010

[2] Sachin Jain, Vivek Agarwal: "A Single-Stage Grid Connected Inverter Topology for Solar PV Systems With Maximum Power Point Tracking", IEEE Vol.22, No.5, pp.1928-1940, 2007

[3] Liqin Ni, Dean J. Patterson, Jerry L. Hudgins: "High Power Current Sensorless Bidirectional 16-Phase Interleaved DC-DC Converter for Hybrid Vehicle Application", IEEE Vol.27, No.3, pp.1141 – 1151, 2012

[4] Koichi Matsu-ura, Koji Orikawa, Jun-ichi Itoh: "Reduction of a boost inductance using a switched capacitor DC-DC converter", IEEE ECCE 2011, pp.1315 – 1322, 2011

[5] Satoshi Miyawaki, Jun-ichi Itoh, Kazuki Iwaya: "Experimental investigation and loss calculation for a bi-directional isolated DC/DC converter using series voltage compensation", APEC 2013, pp.1931-1938, 2013

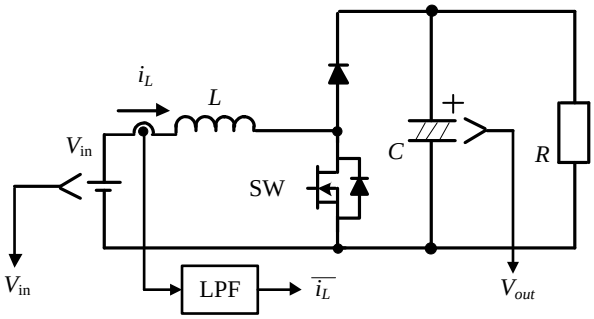

Fig. 15. Boost converter for AVR Experiment.

TABLE III
Experimental Parameters

Input voltage V_{in}	40 V
Output voltage V_{out}	70 V
Rated output power P_{out}	49 W
Boost chopper inductor L	180 μH
Smoothing Capacitor C	680 μF
Switching frequency f_{sw}	50 kHz
Sampling frequency f_{samp}	50 kHz
LPF cutoff frequency f_{cutoff}	5 kHz
Damping factor ζ ACR	0.7
Natural angular frequency ω_n ACR	3000 rad/s
Damping factor ζ AVR	0.7
Natural angular frequency ω_n AVR	300 rad/s

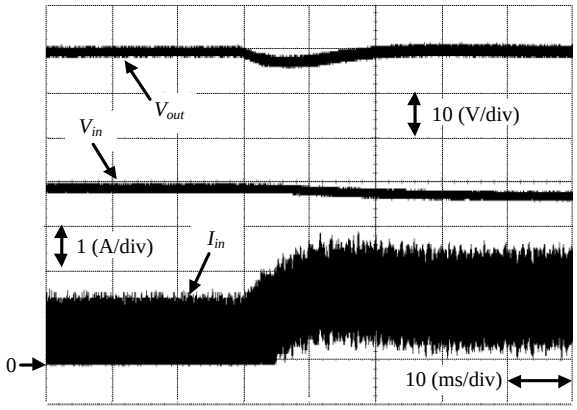

(a) From 40% load in DCM to 100% load in CCM.

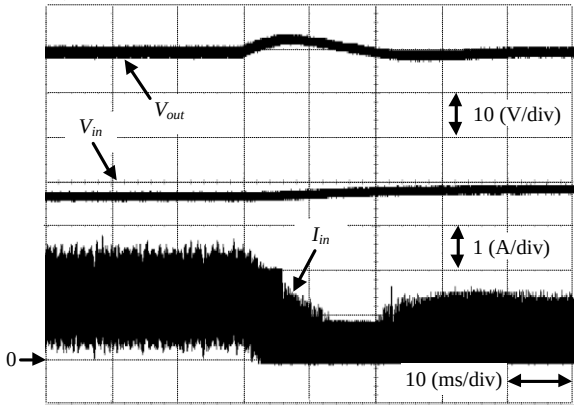

(b) From 100% load in CCM to 40% load in DCM.

Fig. 16. Experimental results of load transient response from 40% load in DCM to 100% load in CCM and vice versa. With the proposed current control method, the input current smoothly alternates between CCM and DCM, so this ensures the stability of the output voltage regulation when load varies.

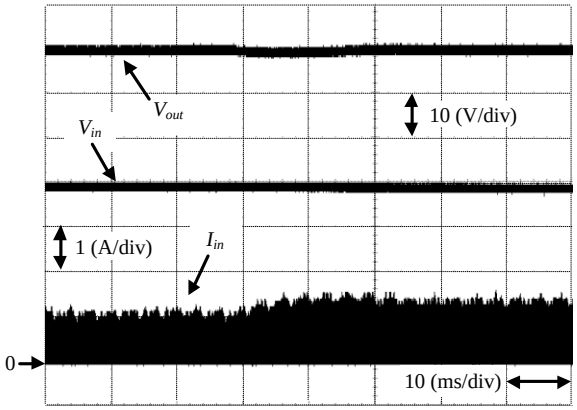

(a) From 20% load in DCM to 40% load in DCM.

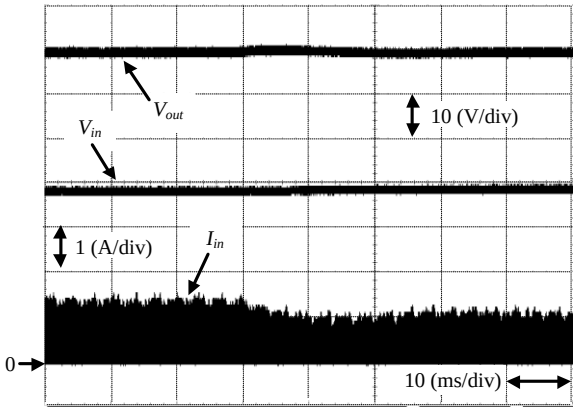

(b) From 40% load in DCM to 20% load in DCM.

Fig. 17. Experimental results of load transient response from 20% load in DCM to 40% load in DCM and vice versa. With the proposed current control method, the input current in DCM is controlled exactly to the conventional CCM, so this ensures the stability of the output voltage when load varies.

[6] Robert W. Erickson and Dragan Maksimovic, Fundamentals of Power Electronics, 2nd ed. New York: Springer-Verlag, 2001

[7] Peter Haaf, Jon Harper: "Understanding Diode Reverse Recovery and its Effect on Switching Losses", Fairchild Power Seminar 2007, ppA.23-A.33, 2007

[8] Juan M. Rivas, Olivia Leitermann, Yehui Han, David J. Perreault: "A Very High Frequency dc-dc Converter Based on a Class Φ2 Resonant Inverter", IEEE PESC 2008, pp.1657-1666, 2008

[9] Juan M. Rivas, David Jackson, Olivia Leitermann, Anthony D. Sagneri, Yehui Han, David J. Perreault: "Design Considerations for Very High Frequency dc-dc Converters", IEEE PESC 2006, pp.1-11, 2006

[10] Robert C. N. Pilawa-Podgurski, Anthony D. Sagneri, Juan M. Rivas, David I. Anderson, David J. Perreault: "Very-High-Frequency Resonant Boost Converters", IEEE Vol.24, No.6,pp.1654-1665, 2009

[11] Anthony D. Sagneri, David I. Anderson, David J. Perreault: "Optimization of Integrated Transistors for Very High Frequency DC-DC Converters", IEEE Vol.28, No.7, pp.3614-3626, 2013

[12] Jian Sun, Daniel M. Mitchell, Matthew F. Greuel, Philip T. Krein, Richard M. Bass: "Averaged Modeling of PWM Converters Operating in Discontinuous Conduction Mode", IEEE Vol.16, No.4, pp.482-492, 2001

[13] Miao Zhu, Fang Lin Luo: "Remaining Inductor Current Phenomena of Complex DC–DC Converters in Discontinuous Conduction Mode General Concepts and Case Study", IEEE Vol.23, No.2, pp.1014-1019, 2008

[14] Xiaotian Zhang, Joseph W. Spencer: "Analysis of Boost PFC Converters Operating in the Discontinuous Conduction Mode", IEEE Vol.26, No.12, pp.3621-3628, 2011

[15] Jeffey Morroni, Luca Corradini, Regan Zane, Dragan Maksimovic: "Adaptive Tuning of Switched-Mode Power Supplies Operating in Discontinuous and Continuous Conduction Modes", IEEE Vol.24, No.11, pp.2603-2611, 2009

[16] Jianping Xu, Jinping Wang: "Bifrequency Pulse-Train Control Technique for Switching DC–DC Converters Operating in DCM", IEEE Vol.58, No.8, pp.3658-3667, 2011

[17] Jinping Wang, Jianping Xu: "Peak Current Mode Bifrequency Control Technique for Switching DC–DC Converters in DCM With Fast Transient Response and Low EMI", IEEE Vol.27, No.4, pp.1876-1884, 2012

[18] Yi-Ping Su, Yean-Kuo Luo, Yi-Chun Chen, Ke-Horng Chen: "Current-Mode Synthetic Control Technique for High-Efficiency DC–DC Boost Converters Over a Wide Load Range", IEEE Vol.PP, pp.1-12, 2013

[19] Yu-Kang Lo, Jing-Yuan Lin, Sheng-Yuan Ou: "Switching-Frequency Control for Regulated Discontinuous-Conduction-Mode Boost Rectifiers", IEEE Vol.54, No.2, pp760-768, 2007

[20] Jong-Won Shin, Bo-Hyung Cho: "Digitally Implemented Average Current-Mode Control in Discontinuous Conduction Mode PFC Rectifier", IEEE Vol.27, No.7, pp.3363-3373, 2012

[21] Koen De Gussemé, David M. Van de Sype, Alex P. M. Van den Bossche, Jan A. Melkebeek: "Digitally Controlled Boost Power-Factor-Correction Converters Operating in Both Continuous and Discontinuous Conduction Mode", IEEE Vol.52, No.1, pp.88-97, 2005

[22] Shu Fan Lim, Ashwin M. Khambadkone: "A Simple Digital DCM Control Scheme for Boost PFC Operating in Both CCM and DCM", IEEE Vol.47, No.4, pp.1802-1812, 2011

[23] Tai-Sik Hwang, Sun-Yeul Park: "Seamless Boost Converter Control Under the Critical Boundary Condition for a Fuel Cell Power Conditioning System", IEEE Vol.27, No.8, pp.3616-3626, 2012